

Torque Ripple Minimization in Direct-Drive Systems

F. Aghili and M. Buehler

Dept. of Mechanical Engineering
McGill University
Montréal, QC H3A 2A7, Canada

J. M. Hollerbach

Dept. of Computer Science
University of Utah
Salt Lake City, UT 84112, USA

Abstract

The open-loop torque control of synchronous motors with minimum torque ripple and minimum copper losses is presented. The control problem is viewed as an optimization problem for the nonlinear mapping from desired torque and position to the motor's phase currents. The performance of the controller to produce virtually ripple-free torque and to enhance the precision of position tracking is demonstrated experimentally.

1 Introduction

Precise position tracking is critical in many robotic and automation applications such as arc welding, laser cutting, NC machining, fixture-less assembly, precise indexing, or antenna tracking. Direct-drive motors are ideal candidates for such applications. They can, in principle, substantially improve the positioning precision since they lack the gearbox required in conventional electric drive systems. However, by the same token, direct drive systems are more adversely affected by the motor's torque ripple. Moreover, direct-drive motors suffer from relatively low continuous torque, which is limited by the power loss in the motor's winding. Therefore, direct-drive motors require accurate torque control with minimum power loss. This is the contribution of this paper.

Control approaches for accurate torque production in direct drive systems and their underlying models have been studied by several researchers [11, 18, 4, 15]. Feedback linearization methods were often proposed, for example in [6, 16, 15].

Manzer *et al.* [11] characterized variable-reluctance motors by approximating their flux linkage via piecewise polynomials. Murai *et al.* [12] proposed heuristic commutation for non-sinusoidal flux distribution. Starr *et al.* [14] and Newman *et al.* [13] applied a 2-D lookup table and a multi-variable function to

determine the phase currents of a variable-reluctance motor with respect to position and torque set points. Filicori *et al.* [4] proposed a dynamical torque controller based on a flux observer which minimizes copper losses or the maximum motor-feeding voltage. Le-Huy *et al.* [10, 3] reduces the torque ripple harmonics for brushless DC motor by using several drive current waveforms. The main tool in the control of synchronous motors is a transformation of phase currents via the 'd-q transformation' [9]. Since this transformation linearizes only an ideal motor with perfectly sinusoidally distributed magneto-motive force, another torque set point is cascaded to cancel torque ripples. This method has been successfully implemented on the previous version of our McGill/MIT motor at MIT [7]. Less than $\pm 1Nm$ ripple has been reported, however, in contrast to this paper, no attempt to minimize power dissipation was made. In a previous paper [1], we presented an alternative approach to torque ripple minimization, which was based on linear magnetics only. In contrast, the approach presented here is applicable to nonlinear magnetics as well.

This paper is organized as follows: Section 2 presents an optimal nonlinear mapping (commutation law) from desired torque and position to motor phase angles with minimum copper losses. This mapping is available in closed form for linear magnetics. In Section 3, the experimental hydraulic dynamometer testbed is described, and the phase torque-angle and torque-current characteristics are identified experimentally for the McGill/MIT synchronous direct-drive motor. The performance of the proposed commutation to produce virtually ripple-free torque and to yield precise position tracking is demonstrated in Section 4 experimentally.

2 Look-Up Table Based Commutation

In this section, we derive the optimal phase currents which minimize both the torque ripple, as well

as the power losses, first for nonlinear, then for linear magnetics. It is assumed that there is negligible cross-coupling between the phase torques [10, 2, 15]. In addition, we assume that the phase currents can be controlled accurately and instantaneously.

2.1 Nonlinear Magnetic Regime

The torque developed by a single phase is a function of the phase current x_j and the (angular motor) position θ . As in related work [17, 13, 7], we assume that this function has separable current and position dependent nonlinearities, as follows,

$$\tau_j(x_j, \theta) = u(x_j) v_j(\theta) \quad j = 1, 2, \dots, p \quad (1)$$

where p is the number of phases (typically $p = 3$), $u(\cdot)$ captures the current nonlinearity due to magnetic saturation and $v_j(\cdot)$ is the position nonlinearity associated with the j th phase. $v_j(\cdot)$ is a periodic function of the motor position, θ , which has some zeros where no torque is generated. However, this problem is eliminated since electric motors have several phases which permits torque-sharing. The motor torque τ is the superposition of all phase torque contributions,

$$\tau = \sum_{r=1}^p u(x_r(\theta, \tau^*)) v_r(\theta). \quad (2)$$

The commutation problem is to solve the above equation in terms of current, $x_r(\theta, \tau^*)$, as a function of motor position, given a desired motor torque τ^* .

Given a scalar torque set point, (2) permits infinitely many (position dependent) phase current wave forms. Since the continuous mechanical power output of electrical motors is limited primarily by heat generated from internal copper losses, it makes sense to use the freedom in the phase current solutions to minimize power losses,

$$P_{loss} = R \sum_{r=1}^p x_r^2(\theta, \tau^*), \quad (3)$$

where R is the armature resistance.

Now by setting $\tau = \tau^*$ in (2), the problem of finding phase currents, x_r , that minimize power losses is formulated by,

$$\begin{aligned} \min \quad & f(\mathbf{x}) \triangleq \sum_{r=1}^p x_r^2 \\ \text{s. th.} \quad & h(\mathbf{x}) \triangleq \tau^* - \sum_{r=1}^p u(x_r(\theta, \tau^*)) v_r(\theta) = 0, \end{aligned} \quad (4)$$

where $\mathbf{x} = [x_1, x_2, \dots, x_p]^T \in \mathbb{R}^p$ is the vector of design variables. θ and τ^* are the system parameters which are also the argument of the optimal solution. Following the Lagrange multiplier approach, we have to solve

$$\nabla f(\mathbf{x}) + \mu \nabla h(\mathbf{x}) = 0. \quad (6)$$

Substituting f and h from (4) and (5) into (6), we obtain

$$2x_j - \mu \frac{du(x_j)}{dx_j} v_j = 0 \quad j = 1, 2, \dots, p \quad (7)$$

and hence

$$\int_0^{x_j} \left(2\zeta - \mu \frac{du(\zeta)}{d\zeta} v_j \right) d\zeta = 0, \quad \text{and} \quad u(0) = 0.$$

It follows that

$$u(x_r) v_r = \frac{x_r^2}{\mu} \quad r = 1, 2, \dots, p. \quad (8)$$

Substituting $u(x_r) v_r$ from (8) into the torque equation (5) yields

$$\mu = \frac{1}{\tau^*} \mathbf{x}^T \mathbf{x}. \quad (9)$$

It is evident from (9) that $\mu = 0$ if all torque functions $x_r(\theta)$ had the same zero crossing which is not the case in multi-phase motors. Thus $\mu \neq 0$, which satisfies the necessary condition for optimality.

Now substituting the Lagrange multiplier from (9) into (8), we obtain p nonlinear equations in p unknowns (x_1, \dots, x_p) ,

$$\begin{aligned} v_1(\theta) \mathbf{x}^T \mathbf{x} - \tau^* \mathcal{J}(x_1) &= 0 \\ v_2(\theta) \mathbf{x}^T \mathbf{x} - \tau^* \mathcal{J}(x_2) &= 0 \\ &\vdots \\ v_p(\theta) \mathbf{x}^T \mathbf{x} - \tau^* \mathcal{J}(x_p) &= 0, \end{aligned} \quad (10)$$

where

$$\mathcal{J}(x_j) \triangleq \frac{x_j^2}{u(x_j)}.$$

Since neither the input functions nor the solution are given in a closed form, discrete functions $x_j(\theta, \tau^*)$ should be numerically obtained over finite numbers of θ and τ^* . It is worth noting that though the torque function is separated with respect to the variables, the optimal current function is not, in general. Therefore, $x_j(\theta, \tau^*)$ must be represented in the form of a two-dimensional look-up table including all cross terms.

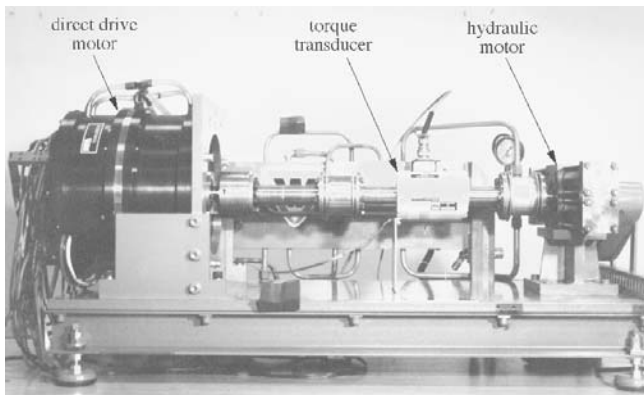


Figure 1: Hydraulic dynamometer testbed.

2.2 Linear Magnetic Regime

For linear magnetics where $u(x_j) = x_j$ and $\mathcal{J}(x_j) = x_j$, the set of equations in (10) are greatly simplified. Now the optimal solution can be expressed explicitly in closed form,

$$x_j(\theta, \tau^*) = \tau^* x'_j(\theta) = \tau^* \frac{v_j(\theta)}{\sum_{r=1}^p v_r^2(\theta)} \quad j = 1, 2, \dots, p. \quad (11)$$

It is worth noting that the denominator in (11) is constant for a three phase motor with perfectly sinusoidal torque functions

$$\begin{aligned} \sum_{r=1}^3 v_r^2(\theta) &= \hat{v}^2 \left(\sin^2(q\theta + \varphi) + \sin^2\left(q\theta + \varphi + \frac{2\pi}{3}\right) \right. \\ &\quad \left. + \sin^2\left(q\theta + \varphi + \frac{4\pi}{3}\right) \right) = \frac{3}{2} \hat{v}^2. \end{aligned}$$

Therefore, each commutation function has the identical wave-shape as its torque function does, i.e., a sinusoidal function with the same phase shift φ .

3 Experimental Phase Torque Characteristics

3.1 Experimental Setup

Fig. 1 illustrates the experimental setup. The direct-drive motor and a hydraulic rack and pinion rotary motor (Parker 113A129BME) are mounted on the rigid structure of the dynamometer. The hydraulic motor's shaft is connected to that of the direct drive motor via a torque transducer (Himmelstein MCRT 2804TC) by means of two couplings (Gam/Jakob

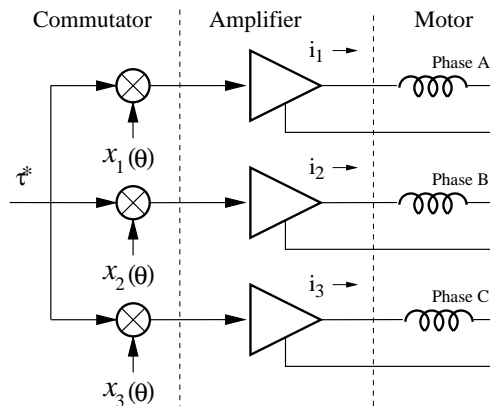


Figure 2: The schematic of motor torque control.

KSS-450) which relieve bending moments or shear forces due to small axes misalignments. The speed of the hydraulic motor is controlled by a pressure compensated flow control valve (Parker TPCS600S01). The hydraulic pressure is set sufficiently high so that the hydraulic actuator regulates the angular speed regardless of the applied direct-drive motor torque. The motor torque is measured in a quasi-static condition, where the motor velocity is kept sufficiently low $1 \frac{deg}{s}$, to ensure that the inertial torque does not interfere with the measurement. An adjustable cam and two limit switches detect the two rotational extremes and activate a solenoid valve through a PLC unit (not shown) to reverse the direction.

The torque control system consists of three main functional components: position sensor, processor unit and power amplifier (Fig. 2). The position sensor is an optical encoder (Teledyne Gurley 8321-4500-CBQANB) mounted to the McGill/MIT motor [5] shaft. Its mechanical resolution of 4,500 lines per revolution is extended 80 times by an electronic interpolator (Teledyne Gurley HR2-20WB-BRD) for 0.001° resolution. The processor unit, an IBM compatible PC based on Intel 80486 processor produces in real time the set points for the three phase current amplifiers. This involves looking up the proper set point value from the look up table, as a function of the motor position, θ , and the desired motor torque, τ^* , and adding the compensating torque (12). Three independent current servo amplifiers (Advanced Motion Control 30A20AC) control the motor's phase currents as specified by the processor. The amplifier's rated current and voltage are 15A and 190V with a switching rate of $22kHz$. Line isolation for the amplifier control inputs is provided by opto-couplers which also eliminate ground loops.

3.2 Friction and Cogging Torques Compensation

In practice, cogging and friction torques act as disturbances and often cannot be neglected. The cogging torque $\tau_{cog}(\theta)$ is due to saliency of the rotor or residual magnetization in stator armatures. The friction torque arises in the motor bearings and consists of viscous and dry friction. Since direct-drive motors operate at relatively low speed dry friction, τ_f , dominates. Although our experiments showed that friction torque is relatively low, we measure and compensate both friction and cogging torques for more accurate torque generation, via

$$\tau_{comp}(\theta, \dot{\theta}) = \tau_{cog}(\theta) + \tau_f \text{sgn}(\dot{\theta}). \quad (12)$$

Cogging torque is a position dependent function which is illustrated in Fig. 3(top). The dry friction torque was evaluated from the difference of the averaged friction torque during clock wise and counter clock wise rotation and turned out to be $\tau_f = 1Nm$.

3.3 Torque-Angle Relationship

The torque trajectory versus position was recorded during rotation, while one phase was energized with a current of 8 A. The three phases' torque-angle profiles, with friction and cogging torques subtracted, are shown in Fig. 3 (bottom). Since our motor torque is linear in terms of current, we can use (11) to calculate the optimal current-position wave shape based on the torque-position measurement. Since the motor has 9 pole pairs, the torque trajectory is periodic in position with a fundamental spatial-frequency of 9 *cpr* (cycles/revolution) and thus the torque pattern repeats every 40 degrees.

The discrete Fourier series coefficients of the torque-position function is shown in Fig. 4. The frequency contents are expressed in harmonics of 9 *cpr*, i.e. the spatial frequency of the 11th harmonics is 99 *cpr*. The figure reveals that the significant frequency components appear at the 1st, 11th and 13th harmonics.

3.4 Torque-Current Relationship

Graphical representation of the torque-current relationship over all positions requires a large number of plots. This is greatly simplified in the frequency-domain because of the small numbers of harmonics.

Similar to the previous experiment, torque-angle is recorded within almost one rotation while the phase current is constant. But the current is incremented at

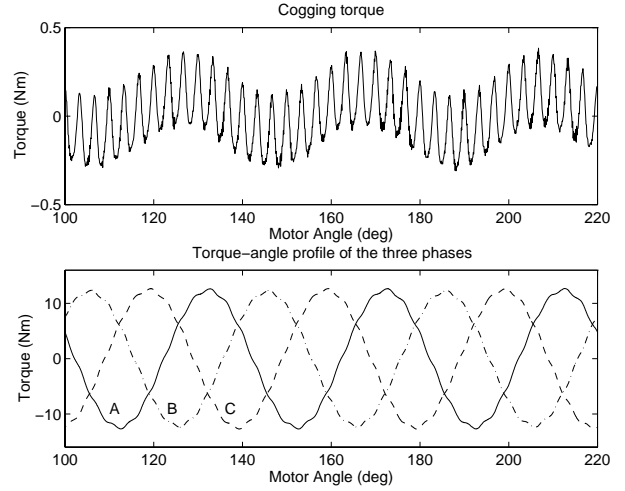


Figure 3: Cogging torque (top), torque-angle profiles (bottom): experimental data.

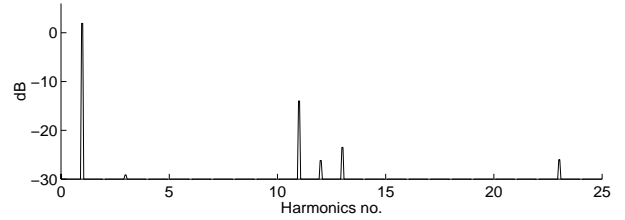


Figure 4: The torque spectrum derived from experimental data

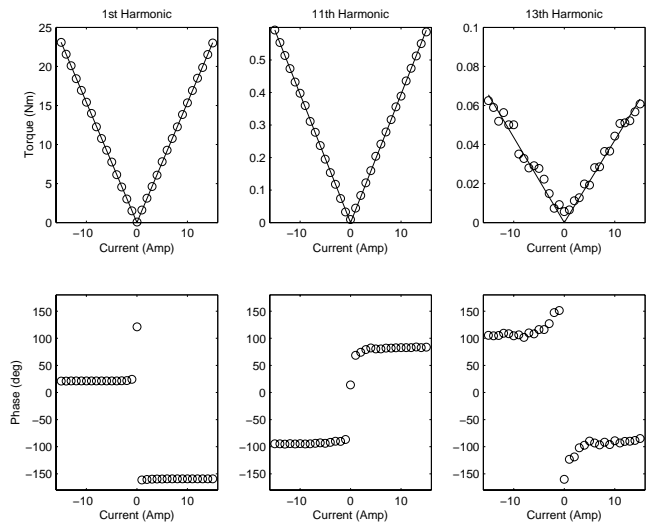


Figure 5: The magnitude and phase of torque harmonics versus phase current: experimental data.

the end of each rotation stroke by 1A until an ensemble of torque profiles belonging to the span of $[-15, 15]$ A is obtained. The major torque harmonics identified from the previous experiment are plotted versus current, Fig. 5. It is evident from this figure that all harmonics have a linear relationship with current. The poor deterministic behaviour of the 13th harmonics is due to its low amplitude which results in a poor S/N torque signal. It can be concluded from the experimental results that the torque is a linear function of current for this particular motor, and the motor operates far from magnetic saturation.

4 Performance Test

4.1 Torque Ripple

The torque controller designed based on the linear magnetic model was tested on the dynamometer. The motor shaft is rotated by the hydraulic actuator while the motor torque is monitored by the torque transducer. Fig. 6 shows the motor torque versus position when sinusoidal and the minimum ripple commutation are applied. A comparison of the torque ripples in the two cases shows the superior performance of our commutation.

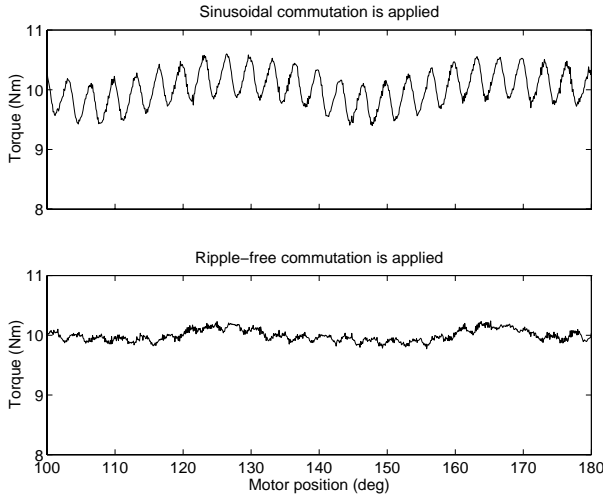


Figure 6: Motor torque in sinusoidal and the ripple free commutations: experimental data.

4.2 The Effect of Torque Ripple in Motion Control

How important is the torque ripple for stability and tracking performance of a motion controller? With a

linear plant and motion controller, the actuator torque ripple includes a decentralized memoryless nonlinearity, i.e. a nonlinear mapping, into the feedback loop. This kind of nonlinearity satisfies the so-called sector condition [8], and therefore, Popov's criterion [8] can be used to assert the stability of the closed loop system. Suppose α_r is the ripple fraction, then the corresponding nonlinearity belongs to the sector $[-\alpha_r, \alpha_r]$ or equivalently $[0, 2\alpha_r]$. Based on Popov's criterion, one can show that for a stabilizing PD or PID position controller, the overall system is absolutely stable for all nonlinearities in $[0, 1]$ [8]. This implies that the actuator torque ripple is not a critical issue for stability. However, the nonlinearity adds perturbation into the system which degrades the tracking performance of the control system.

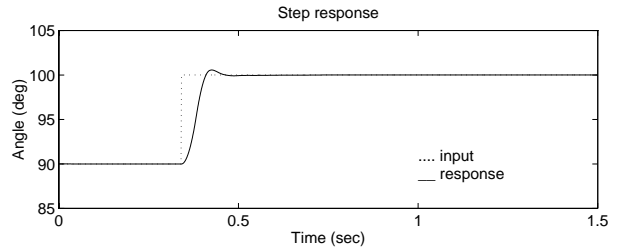


Figure 7: Step response of the position controller: experimental data.

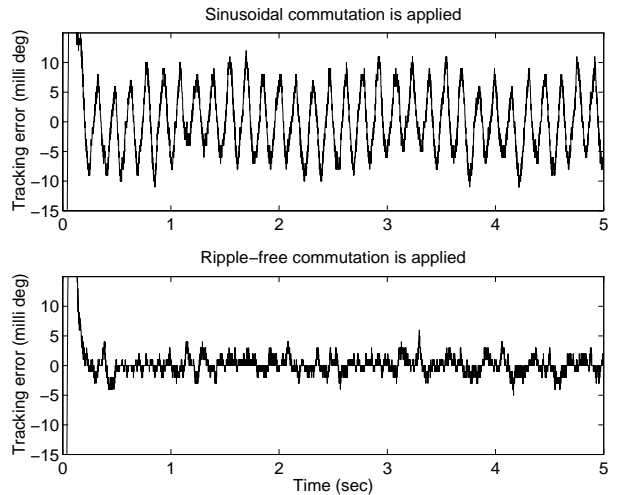


Figure 8: Position tracking errors: experimental data.

We demonstrate the accuracy of position tracking of our direct drive system with and without torque ripple. To this end, a critically damped PID position

controller (Fig. 7) with

$$K_P = 30 \frac{Nm}{deg}, K_I = 200 \frac{Nm}{deg.s}, K_D = 0.65 \frac{Nm.s}{deg}$$

is implemented, in addition to the torque controller. Fig. 8 illustrates the tracking error of the system to a ramp input when the sinusoidal (top) and the minimum ripple (bottom) commutations are applied. The figure clearly shows that the tracking error limited by the torque ripple. In the absence of actuator torque ripples, the tracking error is reduced down to about the encoder resolution (0.001 deg).

5 Conclusion

The motor torque control problem was viewed as the optimization of a nonlinear mapping from commanded torque and motor position to commanded phase current while the redundancy of the problem was exploited to minimize copper losses. The mapping was presented implicitly by calculating the point-to-point values of the current phases versus torque set-point and position for a class of electric machines with separable position and current nonlinearities while an explicit form was presented for linear magnetic systems. A real-time algorithm has been implemented for our direct drive system. Experimental results demonstrated that torque-ripple is almost eliminated. How much torque ripple affects the accuracy of position controllers is also investigated experimentally. It has been shown that we can achieve 0.003 degree accuracy in position tracking when the proposed commutation is used.

Acknowledgements

This project was supported in part by the PRE-CARN TDS Project, through MPB Technologies of Montréal, Québec.

References

- [1] F. Aghili, M. Buehler, and J. M. Hollerbach. Optimal commutation laws for torque control of synchronous motors. In *American Control Conference*, Jun 1997.
- [2] D. Chen and B. Paden. Adaptive linearization of hybrid step motors: stability analysis. *IEEE Trans. Automatic Control*, 38(6):874–887, June 1993.
- [3] E. Favre, L. Cardoletti, and M. Jufer. Permanent-magnet synchronous motors: A comprehensive approach to cogging torque suppression. *IEEE Trans. Industry Applications*, 29(6):1141–1149, 1993.
- [4] F. Filicori, C. G. Lo Bianco, and A. Tonielli. Modeling and control strategies for a variable reluctance direct-drive motor. *IEEE Trans. Industrial Electronics*, 40(1):105–115, 1993.
- [5] J. M. Hollerbach, I. Hunter, J. Lang, S. Umans, and R. Sepe. The McGill/MIT Direct Drive Motor Project. In *Proc. IEEE Int. Conf. Robotics and Automation*, pages 611–617, May 1993.
- [6] M. Ilic'-Spong, R. Marino, S. M. Peresada, and D. G. Taylor. Feedback linearizing control of switched reluctance motors. *IEEE Trans. Automatic Control*, AC-32(5):371–379, 1987.
- [7] D.K. Jackson. Torque-ripple compensation for an axial-air gap synchronous motor. M.Eng. Thesis, M.I.T., Aug. 1994.
- [8] H. K. Khali. *Nonlinear Systems*. Macmillan Publishing Co., 1992.
- [9] P. C. Krause. *Analysis of electric machinery*. McGraw-Hill, 1986.
- [10] H. Le-Huy, R. Perret, and R. Feuillet. Minimization of torque ripple in brushless dc motor drives. *IEEE Trans. Industry Applications*, pages 748–755, 1986.
- [11] D. G. Manzer, M. Varghese, and J. S. Thorp. Variable reluctance motor characterization. *IEEE Trans. Industrial Electronics*, 36(1):56–63, 1989.
- [12] Y. Murai, Y. Kawase, K. Ohashi, and K. Okuyama. Torque ripple improvement for brushless dc miniature motors. *IEEE Trans. Industry Applications*, 25(3):441–449, 1993.
- [13] W. S. Newman and J. J. Patel. Experiments in torque control of the adept-one robot. In *Proc. IEEE Int. Conf. Robotics and Automation*, pages 1867–1872, April 1991.
- [14] G. P. Starr and C. W. Wilson. *Design of a torque control for Adept-2 robot*. ASME, N.Y., 1990.
- [15] D. G. Taylor. Nonlinear control of electric machines: An overview. *IEEE Control Systems*, 14(6):41–51, 1994.
- [16] D. G. Taylor, M. Ilic'-Spong, R. Marino, and S. Peresada. A feedback linearizing control for direct-drive robots with switched reluctance motors. In *Proc. IEEE Int. Conf. Decision and Control*, Miami Beach, Dec 1986.
- [17] F. J. Vallese. *Design and Operation of High-Power Variable Reluctance Motor Based Drive Systems*. PhD thesis, MIT, March 1985.
- [18] R. S. Wallace and D. G. Taylor. Low-torque-ripple switched reluctance motors for direct-drive robotics. *IEEE Trans. Robotics and Automation*, 7(6):733–742, 1991.